Tunnel spin polarization of Fe/MgO/Si contacts reaching 90% with increasing MgO thickness

A. Spiesser, H. Saito, S. Yuasa, and R. Jansen

National Institute of Advanced Industrial Science and Technology (AIST), Spintronics Research Center, Tsukuba, Ibaraki 305-8568, Japan

(Received 27 February 2019; revised manuscript received 2 May 2019; published 25 June 2019)

Using nonlocal spin-transport devices, the tunnel spin polarization (TSP) of Fe/MgO tunnel contacts on Si is determined as a function of the thickness of the MgO. The TSP, extracted from the magnitude of the nonlocal spin-valve and Hanle signals, increases with MgO thickness and is shown to reach values of around 90% at low temperatures. Such a near-perfect spin polarization of the tunnel current indicates that symmetry-based spin filtering due to coherent tunneling occurs in Fe/MgO tunnel contacts on Si, despite the significant lattice mismatch. For MgO thicknesses below 1 nm, the TSP drops unexpectedly rapidly (to values below 25%), which is attributed to the lower crystalline quality of thin MgO layers. In fact, the data suggest that the first 0.7 nm of MgO on the Si contributes very little to the spin filtering.

DOI: 10.1103/PhysRevB.99.224427

I. INTRODUCTION

The discovery [1] of large room-temperature tunnel magnetoresistance (TMR) in magnetic tunnel junctions made from amorphous Al_2O_3 and transition-metal ferromagnets has been paramount to the success of spintronics. It triggered a worldwide search for materials with even higher TMR, and led to the prediction of giant TMR in crystalline Fe/MgO/Fe tunnel structures [2,3]. The giant TMR, predicted to be well over 1000%, was shown to originate from symmetry-based spin filtering, in which states of a certain symmetry in the ferromagnet (FM) couple to evanescent states of the same symmetry in the tunnel barrier, highlighting the importance of the complex band structure of the crystalline tunnel barrier [2,3]. Symmetry-based spin filtering requires highly crystalline structures in which tunneling is coherent so that states of different symmetry cannot couple to each other. Indeed, the subsequent experimental observation of giant TMR in crystalline Fe/MgO/Fe structures [4,5] confirmed this picture and paved the way to the successful application [6–10] of MgO-based tunnel junctions in read heads of high-density magnetic recording systems and as nonvolatile storage elements in magnetic random-access memories. The MgO-based tunnel junctions are also employed in high-frequency oscillators [11], random number generators [12], and neuromorphic computing [13]. After the initial discovery [4,5], in which TMR values of about 200% at room temperature were reported, the TMR values have steadily been improved by tailoring the ferromagnetic materials and perfecting the junction fabrication process [6]. Postdeposition annealing [4,5] improves the crystalline quality of the MgO and the ferromagnetic electrodes and thereby the TMR, although Mn diffusion [14,15] from the antiferromagnetic layer in the junction stack limited the annealing temperature to 350–400 °C. In tunnel junctions containing no Mn, annealing to temperatures around 500 °C resulted in the observation [15,16] of TMR values up to 600% at room temperature, and 1140% at low temperature (5 K), approaching the values predicted by theory [2,3]. Equally important, large TMR values were also achieved in junctions with ultralow resistance-area product [17].

Inspired by this success, crystalline MgO has also widely been used in semiconductor spintronic devices. The application of a charge current across a FM/MgO/semiconductor tunnel junction results in spin injection into the semiconductor, because the rate of injection is spin dependent. This is parametrized by the tunnel spin polarization (TSP), defined as $P_G = (G^{\uparrow} - G^{\downarrow})/(G^{\uparrow} + G^{\downarrow})$, with $G^{\uparrow}$ and $G^{\downarrow}$ the tunnel conductance for majority and minority spin electrons, respectively. In GaAs/AlGaAs spin-light emitting diodes with a Fe/MgO/GaAs spin injector, a TSP of the injected current of about 50% at 100 K was extracted from the polarized electroluminescence [18]. In four-terminal nonlocal spin transport devices with GaAs or Si as the nonmagnetic channel, Fe/MgO tunnel contacts are used not only for spin injection into the semiconductor channel, but also for the electrical detection of the resulting spin accumulation in the channel. Focusing on Si, initially the values of the TSP for the Fe/MgO/Si contacts extracted from spin transport in nonlocal devices were quite small and below 10% at low temperature [19–23]. More recently, higher values have been obtained [24–26], and the largest TSP achieved so far [27] amounts to 53% at low temperature and 18% at room temperature.

Although one may expect that MgO-based tunnel contacts support a very high spin polarization of the tunnel current, one has to keep in mind that there are fundamental differences as compared to the TMR in Fe/MgO/Fe magnetic tunnel junctions. First of all, in the magnetic tunnel junction, both electrodes are ferromagnetic and have spin-dependent states with different symmetries. In contrast, in a Fe/MgO/Si structure, the silicon is not ferromagnetic and the states (and their symmetry) are identical for different spin orientations. A second important aspect is that in a magnetic tunnel junction, the TMR is determined by the difference in the tunnel conductance for parallel (P) and antiparallel (AP) alignment of the magnetization of the two FM electrodes, whereas the spin polarization of the tunnel current in a Fe/MgO/Si contact is determined by the difference between the conductance for the majority and the minority spin electrons. The latter is more directly linked to the difference in the rate of decay

 ©2019 American Physical Society

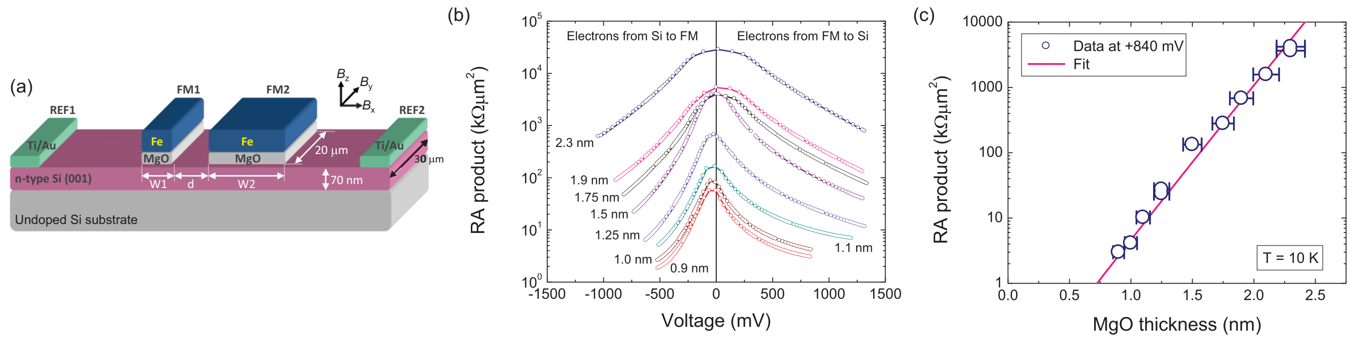

FIG. 1. Device layout and charge transport across the Fe/MgO/Si tunnel contacts. (a) Layout of the nonlocal spin-transport devices, with all the dimensions indicated. (b) Tunnel resistance-area (RA) product of the Fe/MgO/Si contacts as a function of the bias voltage for selected contacts with different MgO thickness, at 10 K. The measurements were performed in the three-terminal configuration, using one of the FM contacts and the two reference contacts REF1 and REF2. Positive bias corresponds to the injection of electron spins from the Fe into the Si channel. (c) Tunnel RA product vs MgO thickness [28] at a bias voltage of +840 mV and at $T = 10$ K. The pink solid line is a fit (as described in the text, Sec. II D).

into the tunnel barrier for states with different symmetry. A third aspect is that the lattices of Si and MgO do not match, and even if the growth is cube-on-cube with a unit cell ratio 4:3, the lattice mismatch is still rather large (3.9%). It remains to be understood how all of this impacts the symmetry-based spin filtering and the maximum obtainable TSP in MgO-based magnetic tunnel contacts on silicon.

Here, we investigate the TSP of Fe/MgO/Si tunnel contacts, and in particular the scaling of the TSP as a function of the thickness of the MgO tunnel barrier. The TSP is extracted from the magnitude of the nonlocal spin-valve and Hanle signals in four-terminal devices with an *n*-type Si channel with a (100) orientation. The TSP increases with MgO thickness and is shown to reach values in the 90–95% range at low temperatures. For MgO thicknesses below 1 nm, the TSP drops unexpectedly rapidly (to values below 25%), which is attributed to the lower crystalline quality of thin MgO layers. In fact, the data suggest that the first 0.7 nm of MgO on the Si contributes very little to the spin filtering. We discuss the role of symmetry-based spin filtering due to coherent tunneling in Fe/MgO tunnel contacts on Si, and the effect of incoherent transport on the TSP.

II. RESULTS

A. Device fabrication and charge transport across the Fe/MgO/Si contacts

The nonlocal spin-transport devices were fabricated on silicon wafers that consist of a 70-nm-thick phosphorous-doped *n*-type Si(001) channel grown epitaxially onto an undoped Si substrate. The Si channel of these wafers, in the as-received state, has a carrier density of 2.7×10^{19} cm^{-3} and a resistivity of 1.3 mΩ cm at 10 K, respectively. The lateral four-terminal devices [Fig. 1(a)] consist of two Fe/MgO electrodes (FM1 and FM2), having widths $W1$ and $W2$ and a gap d, and two reference electrodes (REF1 and REF2) that contact the Si channel at a very large distance (∼100 μm) from the active region of the device where the spin accumulation is created and detected. The Si channel is patterned into a 30-μm-wide strip, and the FM strips have a length of 20 μm. A total of ten devices were fabricated with the thickness t_{MgO} of the MgO barrier varying from 0.75 to 2.3 nm. In order to reduce the device fabrication time, only standard optical lithography was used. The device dimensions are therefore rather large, with most devices having $d = 1.0$ or 1.4 μm, whereas $W1$ and $W2$ are 1.0 and 3.0 μm. We limited the measurements to low temperature ($T = 10$ K), in order to obtain nonlocal spin signals with sufficient signal-to-noise ratio over the full range of MgO thicknesses.

The Fe/MgO tunnel contacts were grown by molecular beam epitaxy (MBE) as follows. First, the Si substrate was cleaned using a so-called RCA process that includes treatments with alkaline (NH_4OH:H_2O_2:H_2O) and acidic (HCl:H_2O_2:H_2O) hydrogen peroxide solutions. This ensures the removal of organic and metallic contaminants and creates a smooth surface. The substrate was then etched in dilute hydrofluoric acid (2%) and rinsed with deionized water to remove the oxide and produce a hydrogen-terminated surface. After introduction into the MBE system having a base pressure in the high 10^{-10}-Torr range, the substrate was annealed at 700 °C for 10 min to desorb the hydrogen and obtain a clean Si surface. The Fe/MgO contacts were grown with an improved process [29]. The MgO layer was deposited in two steps. The first 0.5 nm was grown at 80 °C, then the substrate temperature was raised to 300 °C, and then the remaining part of the MgO was deposited. A 5- or 10-nm-thick Fe layer was then deposited at 90 °C, followed by postdeposition annealing at 250 °C. To protect the tunnel contacts, the sample was covered by a 10-nm-thick Au capping layer.

The charge transport across the contacts was investigated using a three-terminal measurement configuration, applying a current I between one of the two Fe/MgO contacts and reference contact REF1, and measuring the voltage V between the same Fe/MgO contact and reference contact REF2. The tunnel RA product $(V/I) \times A$, with A the area of the Fe/MgO tunnel contact, decays with increasing V [Fig. 1(b)], indicating that the charge transport is nonlinear. The decay of the RA product is faster for negative bias voltage and particularly pronounced for small MgO thickness, whereas the transport is more symmetric for large t_{MgO}. The RA product increases exponentially as a function of t_{MgO}, as expected for tunneling [Fig. 1(c)]. The slope corresponds to about an order

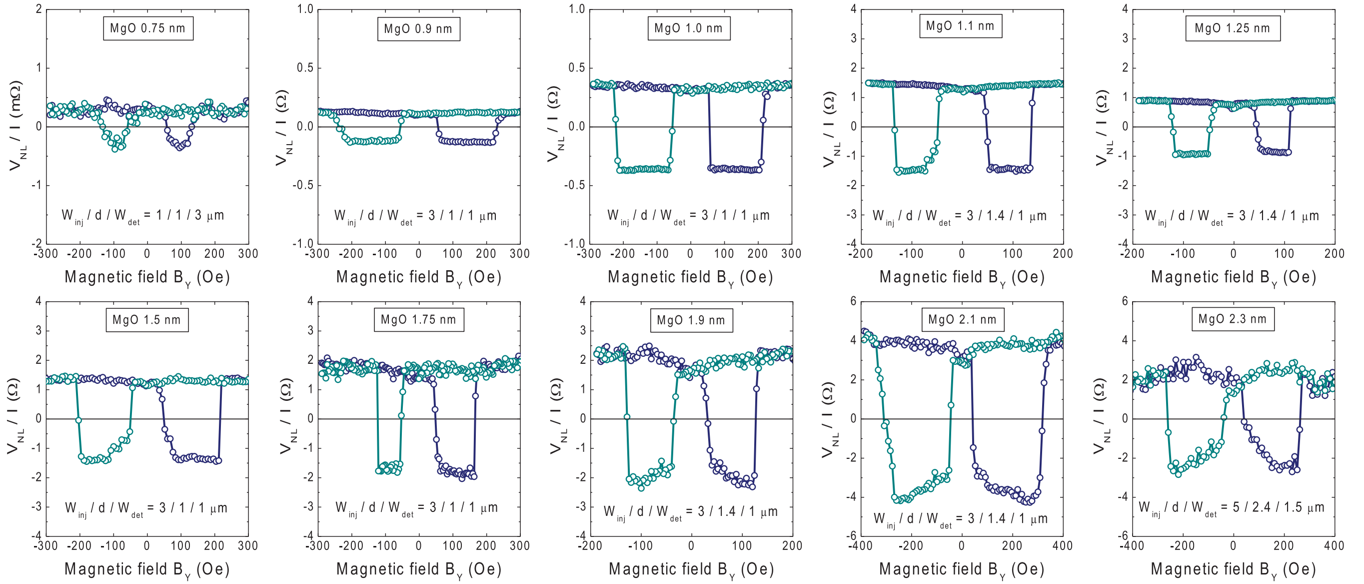

FIG. 2. Selected nonlocal spin-valve signals for devices with different MgO thickness, as indicated in each panel. Also indicated are the widths of the injector W_{inj} and detector W_{det} contact as well as the gap d between them (all in units of μm). The external magnetic field is applied in plane (B_Y) along the long axis of the FM contacts, and swept from plus to minus (green symbols), or in the opposite direction (dark blue symbols). A field-independent offset was subtracted for all curves. For all measurements, a positive current was used, corresponding to injection of electron spins from the Fe into the Si channel. The values of the current are (from small to large MgO thickness) 2.0, 0.5, 0.5, 0.5, 1.5, 1.5, 1.0, 0.17, 0.2, 0.1 mA. The nonlocal voltage V_{NL} was divided by the current and the vertical scales were adjusted for the different devices (also note that the scale is in units of $m\Omega$ for the device with 0.75 nm of MgO). The signal for the device with 2.3 nm of MgO is smaller because the gap and the widths of the electrodes are larger. All data were obtained at $T = 10$ K.

of magnitude per 0.4 nm of MgO. This is comparable to what is observed for metal-based Fe/MgO/Fe tunnel junctions [5].

B. Nonlocal spin transport

The spin current produced by a charge current across the Fe/MgO/Si tunnel junction is measured using the standard four-terminal nonlocal geometry. A constant bias current I is applied between the Fe/MgO contact FM1 and reference contact REF1. This induces a spin accumulation in the Si channel, which spreads out by spin diffusion. A finite spin accumulation is thus produced under the second Fe/MgO contact (FM2) that acts as spin detector and converts the spin accumulation into a charge voltage V_{NL}, that is detected between FM2 and reference contact REF2. The charge current in the detector circuit is kept strictly at zero. The nonlocal voltage V_{NL} is measured as a function of an external magnetic field B_Y applied in the plane of the sample, along the long axes of the FM contacts (y-direction). When the field is swept from plus to minus and back, the relative magnetization of the injector and the detector contact changes between parallel (P) and antiparallel (AP) alignments. Consequently the nonlocal voltage changes sign, producing a spin-valve signal.

Nonlocal spin-valve measurements were performed on one or two different devices for each MgO thickness, using two configurations (either using FM1 and REF1 to apply the current and FM2 and REF2 to detect the nonlocal voltage, or vice versa, using FM2 and REF2 for the current and FM1 and REF1 for the nonlocal detection). Representative nonlocal spin-valve curves are presented in Fig. 2. For all the data, the nonlocal voltage is positive when the magnetization of the two FM contacts is parallel, and negative for the AP state, and sharp transitions occur when the magnetization of either the injector or detector contact is reversed. It was confirmed that the spin signal is genuine and due to spin accumulation in the Si channel and the transport of spins from the injector to the detector, by performing nonlocal Hanle measurements with the magnetic field B_Z applied perpendicular to the magnetization (see Appendix A for an example).

C. Extraction of the tunnel spin polarization

In order to extract the TSP of the Fe/MgO/Si tunnel contacts, we compute the spatial profile of the spin accumulation $\Delta\mu(x)$ induced in the Si channel by spin injection, from the following expression [27] that includes spin diffusion, spin precession, and spin relaxation in one dimension:

$$\Delta\mu(x) = 2e\, J\, P_{\text{inj}}\, r_{\text{ch}} \int_{-W_{\text{inj}}}^{0} \int_{0}^{\infty} \frac{1}{\tau_s} \frac{1}{\sqrt{4\pi D t}} \times \exp\left(-\frac{(x-x_1)^2}{4Dt}\right) \cos\left(\frac{g\mu_B B_Z}{\hbar} t\right) \times \exp\left(-\frac{t}{\tau_s}\right) dt\, dx_1, \tag{1}$$

with P_{inj} the spin polarization of the injected current, D the diffusion constant, τ_s the spin-relaxation time of the Si channel, μ_B the Bohr magneton, e the electron charge, g the electron g factor, $\hbar$ the reduced Planck's constant, and B_Z the magnetic field perpendicular to the spins (in the case of a Hanle measurement). The integration over time t and the

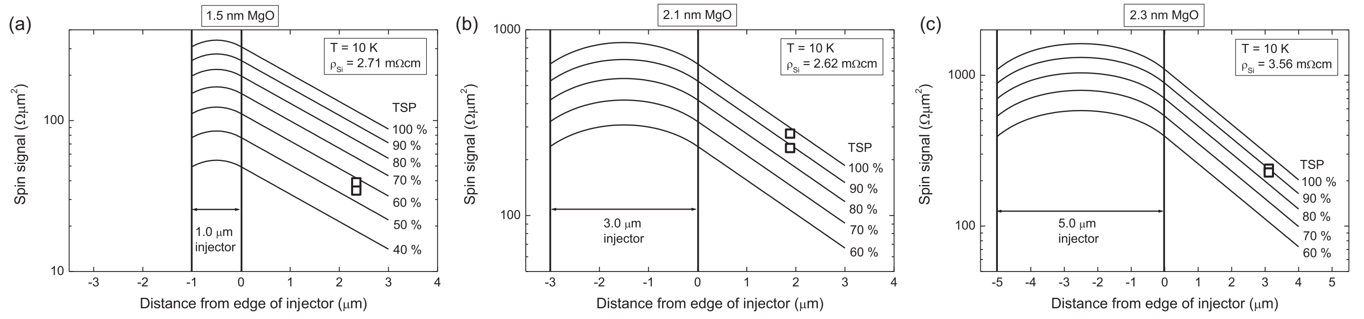

FIG. 3. Determination of the TSP from the measured nonlocal spin-valve signal. (a) Experimental spin signals (symbols) obtained on two devices with 1.5 nm of MgO and $W_{\mathrm{inj}} = 1.0\ \mu$m, $d = 1.0\ \mu$m, and $W_{\mathrm{det}} = 3.0\ \mu$m at 10 K, compared to the signals expected from the calculated spin accumulation profile (solid lines) using $L_{\mathrm{SD}} = 2.4\ \mu$m and different values of the TSP, as indicated (correction factors C_E and $C_{2\mathrm{D}}$ were included). The horizontal scale is the distance from the right edge of the injector, taken to be located at $x = 0$. The experimental data points are placed at position $x = x_c - \Delta x$ (see text), with $\Delta x = 0.154\ \mu$m for a 3-μm-wide detector (see Appendix B). (b) Similar plots for a device with 2.1 nm of MgO and $W_{\mathrm{inj}} = 3.0\ \mu$m, $d = 1.4\ \mu$m, and $W_{\mathrm{det}} = 1.0\ \mu$m. (c) Similar plots for a device with 2.3 nm of MgO and $W_{\mathrm{inj}} = 5.0\ \mu$m, $d = 2.4\ \mu$m, and $W_{\mathrm{det}} = 1.5\ \mu$m. The values of the channel resistivity ρ_{Si} at 10 K, measured in the completed nonlocal device, are also indicated.

width W_{inj} of the injector contact in the x direction yields the spin accumulation at location x in the Si channel produced by spins injected from the injector contact located between $x = -W_{\mathrm{inj}}$ and $x = 0$. Because the thickness of the Si channel ($t_{\mathrm{Si}} = 70$ nm) is much smaller than the spin-diffusion length L_{SD} (2.4 μm at 10 K), the $\Delta\mu$ is constant in the perpendicular z direction. The spin resistance of the channel with resistivity ρ_{Si} is then given by [30,31] $r_{\mathrm{ch}} = \rho_{\mathrm{Si}}\, L_{\mathrm{SD}}(L_{\mathrm{SD}}/t_{\mathrm{Si}})$. The spin accumulation produces a nonlocal voltage given by

$$V_{\mathrm{NL}} = P_{\mathrm{det}} \frac{\Delta\mu(x_c - \Delta x)}{2e} C_E\, C_{2\mathrm{D}} \tag{2}$$

with P_{det} the tunnel spin polarization of the nonlocal spin detector contact having its center at $x = x_c$. This expression deviates from the usual expression [31] in three ways: (i) As explained in Appendix B, when the width of the detector contact is comparable to or larger than L_{SD}, the variation of the spin accumulation as a function of position under the detector needs to be taken into account. The nonlocal voltage should then be evaluated from the spin accumulation at the point with $x = x_c - \Delta x$, which is shifted from the detector center by an amount Δx. (ii) The electric field in the Si channel, produced by the current in the injection part of the nonlocal device, causes spin drift and thereby modifies the spin accumulation under the nonlocal detector, as recently pointed out [32]. This effect has been taken into account by including a correction factor C_E, as described in Appendix C. (iii) The calculation of $\Delta\mu$ uses a one-dimensional approximation [Eq. (1)], which is accurate only if the size W_y of the FM injector and detector contacts in the y direction is very much larger than L_{SD}. We evaluated the error this introduces by performing a calculation in two dimensions, which includes spin diffusion in the orthogonal y direction. The corresponding correction factor $C_{2\mathrm{D}}$ is described in Appendix D. In order to increase the accuracy of the TSP values extracted from the experimental data, these three corrections were taken into account.

By comparing the calculated spin signal to the experimental data, the product $P_{\mathrm{inj}}P_{\mathrm{det}}$ can be determined, because except for P_{inj} and P_{det}, all the parameters are known. As described in Appendix A, Hanle curves measured on the various devices used here are well described using $L_{\mathrm{SD}} = 2.4\pm\ 0.2\ \mu$m and the previously [27] determined value of τ_s (18 ns). From this one also obtains $D = L_{\mathrm{SD}}^2/\tau_s$ (3.2 cm^2/s). For the channel resistivity, rather than using the value obtained from the wafer as received from the supplier, we used the values that were measured in the completed nonlocal devices [33], for each individual device and each MgO thickness. This turned out to be necessary because it was found that after the growth of the tunnel contacts and the device processing, the resistivity of the Si channel had changed, typically by a factor of 2–3 (presumably due to dopant diffusion or segregation during the high-temperature steps in the fabrication process). The resulting values of ρ_{Si} exhibit some variation from device to device, and thus for each device, a slightly different value of the channel spin resistance r_{ch} was used in the calculations.

Figure 3 shows examples of the calculations for three different MgO thicknesses and a width of the injector contact of either 1, 3 or 5 μm. For each case the spin accumulation profile was computed for different values of the TSP between 40 and 100%. This is compared to the experimental data, given by the nonlocal spin signal V_{NL}/I multiplied by the area of the injector contact (solid symbols, which are placed at position $x = x_c - \Delta x$). For 1.5 nm of MgO, the extracted TSP for the two different devices is 54.5 and 58.1%. For the device with 2.1 nm of MgO, TSP values of 88.1 and 96.3% are obtained. For the device with 2.3 nm of MgO, values of 89.9 and 87.8% are obtained.

D. Scaling of the tunnel spin polarization and discussion

Using the procedure described in the previous section, the TSP was obtained for all the devices with different MgO thicknesses [Fig. 4(a)]. For small MgO thicknesses up to 1 nm, the TSP is rather modest and below 25%. However, the TSP increases rapidly as a function of the MgO thickness and, most notably, reaches values in the range of 90–95% for MgO thicknesses above 2 nm. Since, by definition, 100% is the maximum value of the TSP, a near-perfect spin filtering is achieved, corresponding to an almost fully spin-polarized current.

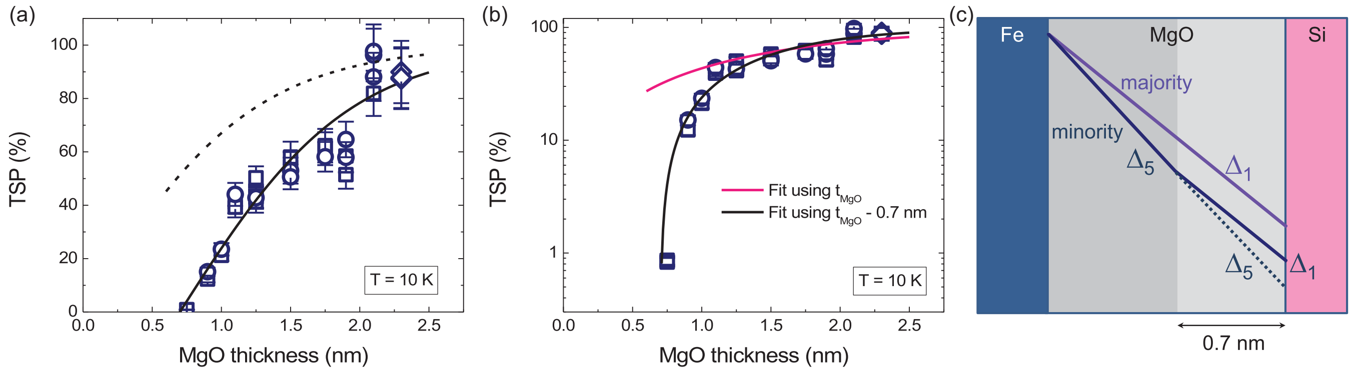

FIG. 4. Scaling of the TSP of Fe/MgO tunnel contacts on Si as a function of the MgO thickness at 10 K. The TSP is plotted on a linear scale (a) or a logarithmic scale (b). Data obtained for different widths of the injector (1.0, 3.0 or 5.0 μm) are presented by a different symbol (squares, circles, and diamonds, respectively). The vertical error bars are determined by the accuracy of the value of L_{SD}. The pink solid line in (b) is a fit using tunnel decay lengths for majority and minority spin of $\lambda_1 = 0.19$ nm and $\lambda_5 = 0.16$ nm, respectively. The black solid lines in (a) and (b) are fits obtained by assuming that 0.7 nm of the MgO does not contribute to the spin filtering (thus subtracting 0.7 nm from t_{MgO}) and using $\lambda_1 = 0.20$ nm and $\lambda_5 = 0.15$ nm. If we use the latter parameters for λ_1 and λ_5 but set the thickness of the inactive MgO layer to zero, the dashed line in (a) is obtained. Panel (c) provides a simplified illustration of the decay of the wave functions for majority and minority spin for a barrier consisting of a crystalline MgO part (dark grey) and a 0.7-nm layer of MgO with poor crystalline quality (light grey).

For metal-based Fe/MgO/Fe magnetic tunnel junctions of high crystalline quality, the observed [4,5] very large values of the tunnel magnetoresistance are known to arise from coherent tunneling and symmetry-based spin filtering [2,3], in which states of a certain symmetry in the FM electrode couple to evanescent states of the same symmetry in the tunnel barrier. The states of Δ_1 symmetry decay relatively weakly into the MgO barrier, whereas states with Δ_5 symmetry decay faster, and states with Δ_2 character decay most rapidly. States with Δ_1 symmetry at the Fermi level of Fe are fully spin polarized and only available for the majority spin, and these dominate the tunneling owing to the weak decay of the Δ_1 states into the MgO. For the minority spin, only states with Δ_5 or Δ_2 symmetry are available, and their contribution to the tunneling decays rapidly with MgO thickness. If tunneling is coherent and states with different symmetry do not couple to each other, the spin polarization increases very rapidly with MgO thickness as the tunnel current becomes dominated by the majority spin Δ_1 states.

We apply the picture of symmetry-based spin-filtering to our case of Fe/MgO tunnel contacts on Si, and compare the predicted scaling of the TSP with MgO thickness to the experimental data. For majority spin electrons, the tunnel current $I^M = I_0 \exp(-t_{MgO}/\lambda_1)$ is determined by electrons with Δ_1 character, with a corresponding decay length λ_1. For minority spin electrons, the tunnel current $I^m = I_0 \exp(-t_{MgO}/\lambda_5)$ is determined by electrons with Δ_5 character, with a corresponding decay length λ_5. The TSP is then given by $(I^M - I^m)/(I^M + I^m)$. The best fit of the data is obtained for $\lambda_1 = 0.19$ nm and $\lambda_5 = 0.16$ nm [pink solid line in Fig. 4(b)], where it should be noted that the value of λ_1 controls the total tunnel current and was chosen so as to simultaneously fit the variation of the tunnel RA product as a function of the MgO thickness [pink solid line in Fig. 1(c)]. It is evident that the model fails to describe the TSP data, and in particular, it does not predict the strong decay of the TSP for very small MgO thicknesses below about 1 nm. It was confirmed that back flow of spins into the FM electrode, which can occur for contacts with small RA product [30,31,34,35], is negligible and does not influence the extracted values of the TSP (see Appendix E).

The fact that the TSP drops to a value smaller than 1% for 0.75 nm of MgO suggests that the first ~0.7 nm of the MgO tunnel barrier does not contribute much to the spin filtering. With this in mind, we used a modified model in which, instead of using the full MgO thickness, we subtract 0.7 nm from t_{MgO}. Indeed, a very satisfactory fit of the data is then obtained, for $\lambda_1 = 0.20$ nm and $\lambda_5 = 0.15$ nm [black solid lines in Figs. 4(a) and 4(b)]. In particular, the sharp drop of the TSP for small t_{MgO} is now properly reproduced. In this modified model it is considered that coherent tunneling and symmetry-based spin filtering does occur in the top part of the MgO, but not in the first 0.7 nm of MgO that is in contact with the Si. This might happen if the first few layers of MgO on Si are of poor crystalline quality. In this case, minority spin electrons of Δ_5 character, after decaying from the Fe through the top part of the MgO, can couple to evanescent states with Δ_1 symmetry in the first 0.7 nm of MgO [as illustrated in Fig. 4(c)]. For minority spins we then have $I^m = I_0 \exp[-(t_{MgO} - 0.7\text{ nm})/\lambda_5] \exp(-0.7\text{ nm}/\lambda_1)$. In this partly coherent scenario, the decay rate for both types of spin is given by λ_1 in the first 0.7 nm of MgO, which then effectively does not contribute to the spin filtering. From this one might also infer that if the crystalline quality of the first 0.7 nm of MgO can be improved so that the full MgO thickness contributes to the spin filtering, the TSP is predicted to increase significantly, especially for small t_{MgO}, as indicated by the dashed line in Fig. 4(a). Values of the TSP around 60% would then become possible for resistance-area products down to a few kΩ μm^2.

Some support for the above interpretation comes from structural characterization of the tunnel contacts by transmission electron microscopy (TEM). For very thin barriers [i.e., 0.9 nm, Fig. 5(a)] areas with crystalline MgO are very rare. For 1.2 nm of MgO [Fig. 5(b)], a larger number of crystalline areas with visible MgO lattice planes can be found, but the barrier is far from fully crystalline. For the thicker tunnel

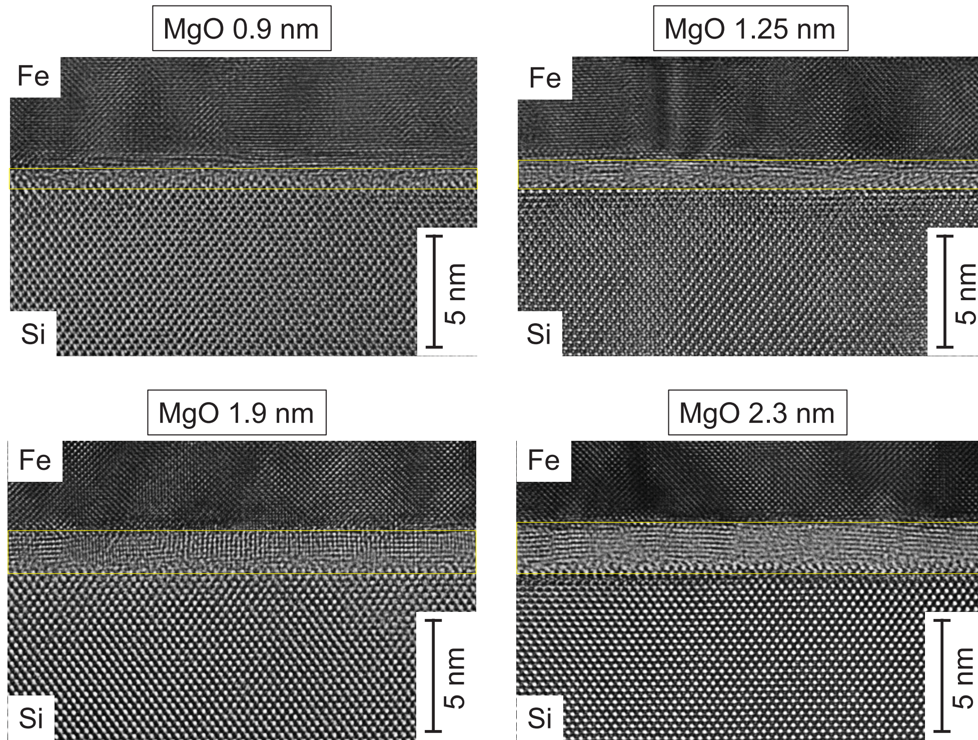

FIG. 5. Cross-sectional TEM images of the Fe/MgO tunnel contacts on Si for four different MgO thicknesses, respectively, 0.9, 1.25, 1.9, and 2.3 nm. The MgO tunnel barrier is indicated by the yellow lines.

barriers [1.9 and 2.3 nm, Figs. 5(c) and 5(d), respectively] most of the tunneling area contains crystalline MgO. However, it can also be seen that most of the crystalline MgO is located in the top part of the barrier (i.e., on the Fe side), and that the MgO lattice planes often do not extend all the way down to the interface with the Si. The first few atomic layers of the MgO on the Si thus appear rather disordered, which may indeed be the origin of the low TSP for small MgO thicknesses. We therefore believe that the partly coherent picture captures the essence of the spin transport in the Fe/MgO/Si tunnel contacts. Nevertheless, the TEM results reveal that a description of the barrier in terms of a fully crystalline MgO part on a fully disordered 0.7 nm of MgO is oversimplified, as some crystalline regions close to the Si interface are present, as well as a significant number of defects and dislocations in the top part of the MgO barrier.

It may be considered as rather surprising that TSP values in the range of 90–95% are observed for MgO barriers thicker than 2 nm, given that the MgO is not perfectly crystalline. To provide some context, a TSP value of 95% in a FM/insulator/FM magnetic tunnel junction would, in a simple Julliere description [36], yield a TMR as large as 1850%. In Fe- or Co-based magnetic tunnel junctions with a fully epitaxial MgO barrier of very high crystalline quality, the TMR values are in the range of 500 to about 1100% at low temperature [6,15,16,37]. We speculate that the effect of disorder on the TMR of a Fe/MgO/Fe junction is not the same as the effect of disorder on the TSP of a Fe/MgO/Si contact. In a Fe/MgO/Fe junction in the AP configuration, majority spin Δ_1 states in one Fe electrode cannot couple to any states in the other Fe electrode because for the AP configuration the relevant states are of minority spin and these have a different symmetry (Δ_5 and Δ_2). Disorder in the tunnel barrier or at the interfaces would enable this coupling and greatly increase the conductance in the AP configuration and thereby strongly reduce the TMR.

In contrast, in a Fe/MgO contact on Si there is only one FM electrode while the electronic states in the Si electrode do not depend on electron spin. Near the Si conduction-band minimum, the states are of Δ_1 symmetry at the center of the surface Brillouin zone, and have mixed character for states with nonzero momentum $k_\parallel$ parallel to the tunnel interface [38]. If transport is fully coherent, minority spin states from the Fe with Δ_5 symmetry cannot propagate into the Si at $k_\parallel = 0$, but they can for nonzero $k_\parallel$. The conductance for the minority spin channel is then determined partially by reflection at the MgO/Si interface (depending on the $k_\parallel$) and partially by the decay in the MgO barrier (decay length λ_5). However, the transport across the MgO/Si interface is not expected to be coherent since the MgO and Si lattices do not match. One may then assume that at the MgO/Si interface, evanescent states of all symmetries in the MgO, for both spins, can couple to the states in the Si. The TSP is then determined exclusively by the different decay lengths in the MgO (λ_1 for majority spins and λ_5 for minority spins). Now, if part of the MgO (e.g., the 0.7 nm on the Si side of the barrier) is disordered, the only effect would be to reduce the effective thickness of the MgO barrier that contributes to the spin-dependent decay. Therefore, the lack of crystalline order in the first ~0.7 nm of the barrier does not make it impossible to reach a TSP of 90–95% (it just shifts the required t_{MgO} to larger values). It would be of interest to further explore

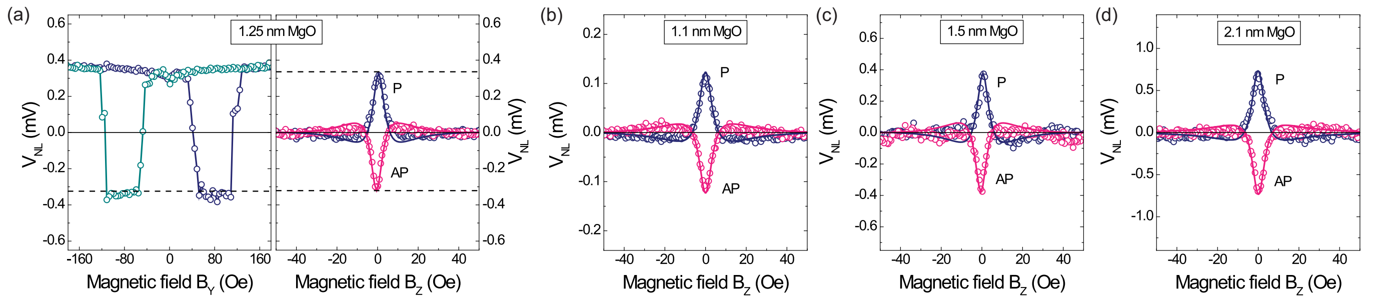

FIG. 6. (a) Nonlocal spin signals V_{NL} measured in the spin-valve geometry (left panel) with the external magnetic field applied in-plane (B_Y), or in the Hanle geometry (right panel) with the field applied perpendicular (B_Z) to the plane of the sample, for a device with 1.25 nm of MgO at 10 K. The current I is +0.3 mA (injection of electron spins from the Fe into the Si channel). The solid lines in the right panel are calculated using $L_{\mathrm{SD}} = 2.2\ \mu$m, $\tau_s = 18$ ns, and the measured value of $\rho_{\mathrm{Si}} = 3.37$ mΩ cm for this device. (b) Nonlocal Hanle signals for a device with 1.1 nm of MgO at 10 K, for $I = +0.1$ mA. The solid lines are calculated using $L_{\mathrm{SD}} = 2.6\ \mu$m, $\tau_s = 18$ ns. (c) Nonlocal Hanle signals for a device with 1.5 nm of MgO at 10 K, for $I = +0.2$ mA. The solid lines are calculated using $L_{\mathrm{SD}} = 2.2\ \mu$m, $\tau_s = 18$ ns. (d) Nonlocal Hanle signals for a device with 2.1 nm of MgO at 10 K, for $I = +0.2$ mA. The solid lines are calculated using $L_{\mathrm{SD}} = 2.4\ \mu$m, $\tau_s = 18$ ns. For all devices, the FM contacts have widths of 1.0 and 3.0 μm and the gap d is 1.4 μm. The 1.0-μm-wide contact was used as the spin injector, except for the device with 2.1 nm of MgO, for which the 3.0-μm contact was used as the injector.

the sensitivity to disorder for the Fe/MgO/Si system using first-principles based calculations of the tunnel transport.

III. SUMMARY

The tunnel spin polarization of Fe/MgO tunnel contacts on Si was determined as a function of the thickness of the MgO. The TSP was extracted from the magnitude of nonlocal spin-valve and Hanle signals. The TSP increases with MgO thickness and reaches values of about 90% for MgO thicknesses above 2 nm at 10 K. Such a near-perfect spin polarization of the tunnel current indicates that symmetry-based spin filtering due to coherent tunneling occurs in Fe/MgO tunnel contacts on Si, even though there is a significant lattice mismatch between the MgO and the Si. For MgO thicknesses below 1 nm, the TSP drops rather rapidly (to values below 25%). This is attributed to the lower crystalline quality of thin MgO layers. The scaling of the TSP with MgO thickness can be well described, including the low thickness range, if it is assumed that the first 0.7 nm of MgO on the Si does not contribute to the spin filtering.

ACKNOWLEDGMENT

This work was supported by the Grant-in-Aid for Scientific Research on Innovative Areas, Nano Spin Conversion Science (Grants No. 26103002 and No. 26103003).

APPENDIX A

In this Appendix we present nonlocal spin-valve and Hanle measurements and determine the value of L_{SD} of the Si, which is needed in order to extract the TSP from the nonlocal spin signals. In previous work [27] on nonlocal devices prepared on the same type of Si wafers, we determined a spin-diffusion length of $L_{\mathrm{SD}} = 2.2\ \mu$m and a spin-relaxation time $\tau_s = 18$ ns. We expected similar values for the devices used in the present study, since these were prepared with a similar process, although some details of the process were slightly different. We therefore performed Hanle measurements on a number of devices and confirmed that these can be described with similar values of L_{SD} and τ_s. Data obtained on a device with 1.25 nm of MgO is shown in Fig. 6(a). The Hanle curves for P and AP alignment of the injector and detector magnetization have comparable amplitude and opposite sign, and the amplitudes of the Hanle signals for P and AP configurations are in agreement with the spin-valve signal, as it should. The solid lines represent the calculated Hanle curves, obtained by numerical evaluation of the spin accumulation at the center of the detector using Eq. (1), as done previously [27]. A satisfactory agreement between the calculated and the measured Hanle curves is obtained using $L_{\mathrm{SD}} = 2.2\ \mu$m and $\tau_s = 18$ ns. Because we found that there is some variation in the resistivity of the Si in the devices used here, we measured Hanle curves on some other devices with different MgO thickness [see Figs. 6(b)–6(d)]. These Hanle curves can be well described by using the same value of τ_s and values of L_{SD} of 2.6, 2.2, and 2.4 μm, respectively, for the devices with 1.1, 1.5, and 2.1 nm of MgO, as indicated by the solid lines in each of the panels. Because there is some variation in the values of L_{SD}, we used $L_{\mathrm{SD}} = 2.4 \pm 0.2\ \mu$m to extract the TSP from the nonlocal spin signals, and translated the uncertainty in the value of L_{SD} into error margins for the TSP, which are included in Fig. 4 (note that in previous work [27], we used nonlocal devices with different spacing and widths to determine L_{SD}, and obtained a value of 2.2 μm with an error margin of $\pm$ 0.2 μm).

We also considered the error that is introduced if the widths of the FM contacts deviate from the values defined by the lithography mask, which can happen if the exposure or etching time is slightly off. However, the error is very small, because the nonlocal voltage depends very weakly on the contact widths if the same current is used. In fact, in the regime where W_{inj} is comparable to or smaller than L_{SD}, the V_{NL} is determined exclusively by the center-to-center distance (which is well defined). We calculated the error produced if the injector and detector contacts are larger or smaller by 0.2 μm (0.1 μm on each side), and found that this changes the extracted value of the TSP by a factor of only 0.99 or 1.01.

APPENDIX B

In this Appendix we describe an exact expression for the voltage detected by a nonlocal spin detector as a function of the width of the detector contact. If the detector width is much smaller than the spin-diffusion length L_{SD}, the usual approximation, in which the voltage is computed from the spin accumulation at the center of the detector contact, is appropriate. However, when the width becomes comparable to or larger than L_{SD}, the spin accumulation is significantly nonuniform under the detector contact. Because the spin accumulation does not vary linearly with distance from the injector, the detected nonlocal voltage no longer corresponds to the spin accumulation at the center of the detector.

In a nonlocal measurement, the *total* charge current I_{det} in the detector circuit is zero, but the local current *density* $J_{det}(x, y)$ does not have to be zero at every position (x, y) in the contact area. Because the local detector current density depends on the local spin accumulation $\Delta\mu(x, y)$, a spatially nonuniform spin accumulation under the detector produces a spatial variation of the detector current density. For a tunnel contact we have, in linear response,

$$J_{det}(x, y) = G[V - (P_G/2)\Delta\mu(x, y)]. \quad \text{(B1)}$$

The tunnel conductance G and the spin polarization P_G of the tunnel conductance are taken to be constant, independent of position. The voltage $V(x, y)$ across the nonlocal detector contact can, in principle, vary with position. However, the detector electrode is usually a highly conductive metal whose resistance square is orders of magnitude smaller than the tunnel resistance-area product of the detector contact. The metal then acts as an equipotential plane and $V(x, y)$ is a constant equal to the detected nonlocal voltage V_{NL}.

We consider a detector having dimensions W_x and W_y in the x and y direction, respectively, with its center located at $x = x_c$. The spin accumulation varies only as a function of the distance x from the edge of the injector contact according to

$$\Delta\mu(x, y) = \Delta\mu^0 \exp\left(-\frac{x}{L_{SD}}\right) \quad \text{(B2)}$$

with $\Delta\mu^0$ the value of the spin accumulation at the edge of the injector, taken to be located at $x = 0$. The total tunnel current in the detector contact is then given by

$$I_{det} = W_y \int_{x_c - W_x/2}^{x_c + W_x/2} J_{det}(x, y)\, dx. \quad \text{(B3)}$$

Inserting Eqs. (B1) and (B2), evaluating the integral, and requiring $I_{det} = 0$ then gives

$$V_{NL} = (P_G/2)\Delta\mu^0 \exp\left(-\frac{x_c}{L_{SD}}\right)\left\{\left(\frac{2L_{SD}}{W_x}\right)\sinh\left(\frac{W_x}{2L_{SD}}\right)\right\}. \quad \text{(B4)}$$

The term in curly brackets is the correction factor that is to be included when the detector width becomes comparable to or larger than L_{SD}. This correction term is unity when $W_x \ll L_{SD}$, in which case the voltage corresponds to the spin accumulation at the center of the detector. For $W_x = L_{SD}$, the correction term is equal to 1.042, and thus the detected voltage is about 4% larger compared to what would be obtained from the spin accumulation at the center of the detector. It can be shown that V_{NL} corresponds to the spin accumulation at the point with $x = x_c - \Delta x$, which is shifted by an amount Δx from the detector center, with

$$\Delta x = \frac{W_x}{2} + \frac{W_x}{\alpha}\ln\left[\frac{1}{\alpha}\left[1 - \exp(-\alpha)\right]\right] \quad \text{(B5)}$$

and $\alpha = W_x/L_{SD}$. Note that only at the point with $x = x_c - \Delta x$ is the local tunnel current density in the detector zero. On one side of this point, $J_{det}(x, y)$ is positive and increases towards the edge of the detector, whereas it is negative on the other side, in such a way that the total detector current is zero. This implies that there is a small current circulating within the detector tunnel contact area. The values of the correction factor and Δx for the nonlocal devices used to extract the TSP of the Fe/MgO contacts are given in Table I.

APPENDIX C

In this Appendix we describe the correction of the TSP value extracted from the nonlocal spin-transport data when the drift electric field E in the Si channel is taken into account. This is especially relevant when the injection current is larger, for which E is appreciable. As we have recently pointed out [32], spin drift due to the nonzero electric field in the injection part of a nonlocal device causes a redistribution of the spin accumulation everywhere in the channel, including under the nonlocal detector, and thus modifies the detected nonlocal voltage. This effect can be taken into account by taking the spin accumulation calculated for purely diffusive transport, and multiplying this by the following correction factor for spin drift [32]:

$$C_E = \frac{2L_{SD}}{L_{SD} + L(E)} \quad \text{(C1)}$$

with $L(E)$ the total spin-transport length that includes spin diffusion as well as spin drift in the Si channel [32,39]:

$$L(E) = \left(\frac{eE}{2\epsilon_d} + \sqrt{\left(\frac{eE}{2\epsilon_d}\right)^2 + \left(\frac{1}{L_{SD}}\right)^2}\right)^{-1}. \quad \text{(C2)}$$

The E is defined [32] to have a negative sign when electrons are injected from the FM into the Si. The value of E is calculated from the injection current, the cross section of the Si channel, and the Si resistivity, which was determined for each nonlocal device. The expression for $L(E)$ contains an energy scale ϵ_d, which, according to the theory [39], is given by eD/μ, with μ the mobility of the Si (179 cm^2/V s at 10 K) and D the diffusion constant of the Si. The latter can be obtained from the measured spin-diffusion length and spin-relaxation time via $D = L_{SD}^2/\tau_s$. One then obtains $\epsilon_d =$ 17.9 meV. However, it was demonstrated [32] that using this theory value of ϵ_d significantly overestimates the effect of spin drift (by about a factor of 3), and that a good match with the measured spin drift is obtained only if the ϵ_d is increased by a factor of about 3. We therefore used a value of 54 meV for ϵ_d. The resulting correction factor is close to unity for the devices with larger t_{MgO}, because the injection current is small. However, for a few of the measurements on devices with smaller t_{MgO}, currents of 1–2 mA were used, for which

TABLE I. Correction factor and Δx for different widths W_x of the detector contact, corresponding to the different nonlocal devices used to extract the TSP of the Fe/MgO tunnel contacts.

W_x (μm)	L_{SD} (μm)	Correction factor $(2L_{SD}/W_x)\sinh(W_x/2L_{SD})$ (dimensionless)	α (dimensionless)	Δx (μm)
1.0	2.4	1.007	0.417	0.017
1.5	2.4	1.016	0.625	0.039
3.0	2.4	1.066	1.25	0.154

C_E is 0.83–0.70, in which case the extracted TSP becomes larger by a factor of up to 1.2.

APPENDIX D

In this Appendix we describe how the spin accumulation calculated from the one-dimensional (1D) spin-transport equations is modified when transport in both the lateral directions (x and y) is taken into account. The two-dimensional (2D) description is relevant because for the devices used here, the width of the Si channel in the y direction (30 μm) is larger than the size ($W_y = 20$ μm) of the FM contacts in the y direction, so that spins injected into the Si channel will also spread out into the y direction. In two dimensions, the expression for the spin accumulation becomes

$$\Delta\mu(x,y) = 2eJP_{\text{inj}}\, r_{\text{ch}} \int_0^{W_y}\int_{-W_{\text{inj}}}^{0}\int_0^{\infty} \frac{1}{\tau_s}\frac{1}{4\pi Dt} \times \exp\left(-\frac{(x-x_1)^2+(y-y_1)^2}{4Dt}\right)\cos\left(\frac{g\mu_B B_Z}{\hbar}t\right) \times \exp\left(-\frac{t}{\tau_s}\right) dt\,dx_1\,dy_1. \quad \text{(D1)}$$

The spin accumulations $\Delta\mu^{2D}$ and $\Delta\mu^{1D}$ calculated for the 2D and the 1D model are compared in Fig. 7. The variation of the spin accumulation in the x direction at the center of the device [along line A depicted in Fig. 7(a)] is very similar for the 2D and the 1D calculation [Fig. 7(b)]. However, when we examine how the spin accumulation under the *detector* contact varies along the y direction [Fig. 7(c)], we find that in the 2D model (i) there exists a nonzero spin accumulation outside the area of the detector contact area, and (ii) there is a sizable decay of the spin accumulation under the detector contact towards the edges of the detector.

Because of the diffusion of spins into the y direction, the nonlocal voltage V_{NL}^{2D} computed for the 2D model will be smaller than the voltage V_{NL}^{1D} for the 1D model by a factor C_{2D}:

$$V_{\text{NL}}^{2D} = C_{2D}\, V_{\text{NL}}^{1D}. \quad \text{(D2)}$$

In order to calculate the correction factor C_{2D}, we note that the 2D spin-accumulation profile under the detector contact is reasonably well described by the following analytical expression [see the solid line in Fig. 7(c)]:

$$\Delta\mu^{2D}(y) = \Delta\mu^{1D}\left[1-\frac{1}{2}\exp\left(-\frac{y}{L_{SD}}\right)\right] \times\left[1-\frac{1}{2}\exp\left(\frac{y-W_y}{L_{SD}}\right)\right]. \quad \text{(D3)}$$

The procedure to calculate the nonlocal potential in the presence of such an inhomogeneous spin accumulation is similar to that described in Appendix B. The inhomogeneous $\Delta\mu$ gives rise to an inhomogeneous detector tunnel current density J_{det}. By integrating J_{det} over the size of the detector in the y direction, using Eq. (D3) for the spin accumulation profile, and requiring that the total detector current is zero, we obtain

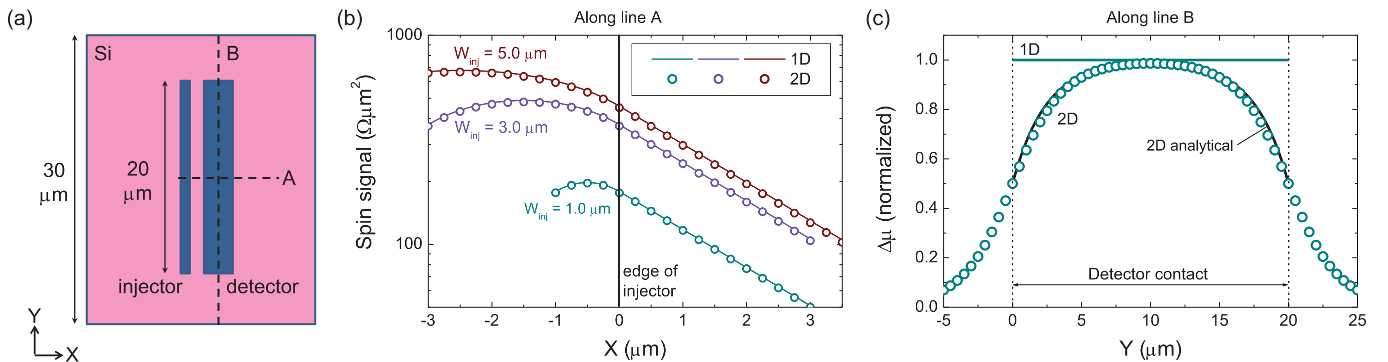

FIG. 7. Spin accumulation profiles for a 2D calculation. (a) Top view of the nonlocal device, with relevant lateral dimensions indicated. The FM contacts are in dark blue, the left FM contact is used as injector, the right contact as nonlocal detector. (b) Comparison of the spin accumulation profile in the x direction along line A depicted in (a), calculated using the 1D model (solid lines) or the 2D description (open circles), for three different widths of the injector contact. (c) Spin accumulation profile in the y direction along line B depicted in (a) for the 1D model (solid green line) or the 2D description (open circles), for $W_{\text{inj}} = 1.0$ μm, $W_{\text{det}} = 3.0$ μm and $d = 1.0$ μm. The edges of the FM strip are located at $y = 0$ and $y = +20$ μm. The black solid line corresponds to the profile obtained from Eq. (D3). A value of 2.4 μm was used for L_{SD}.

V_{NL}^{2D} and from that,

$$C_{2D} = 1 - \frac{L_{SD}}{W_y}, \quad \text{(D4)}$$

in which we have used that $W_y \gg L_{SD}$. The value of C_{2D} is then 0.88. Including this enhances the extracted TSP by a factor of 1.066. It was confirmed that the spin accumulation profile under the detector contact is well described by Eq. (D3) for all the devices with different dimensions and contact spacing used in this work. The same correction factor is thus used for all.

APPENDIX E

In this Appendix it is confirmed that the extracted values of the TSP are not influenced by back flow of spins into the FM electrode (conductivity mismatch [34]). Back flow can occur for tunnel contacts with small RA product when the buildup of a large spin accumulation under the injector contact reduces the spin polarization of the injected current [30,31,34,35]. We use the parameters of the device with the thinnest MgO barrier (0.75 nm) and quantify the reduction of the spin signal due to back flow, which is described [31] by the factor $\mathrm{RA}/[\mathrm{RA} + r_s(1 - \mathrm{TSP}^2)]$. This is unity if the RA product of the tunnel contact is much larger than r_s, the *effective* spin resistance of the Si channel. The latter is equal to $r_{ch} = \rho_{Si} L_{SD}(L_{SD}/t_{Si})$ if the lateral dimensions of the contact are much larger than L_{SD} and also $t_{Si} \ll L_{SD}$. However, for a 1-μm-wide injector contact, the spin accumulation is smaller than for a large contact [27], and so back flow is reduced. This is described by the integral in Eq. (1), that is, the effective spin resistance r_s that controls the back flow is given by r_{ch} times the integral, evaluated at the center of the injector, where the spin accumulation is maximum. For a 1-μm-wide contact this yields $r_s = 0.204 \times r_{ch}$. Using $\rho_{Si} = 2.84\ \mathrm{m}\Omega\,\mathrm{cm}$, $L_{SD} = 2.2\ \mu\mathrm{m}$, and $t_{Si} = 70$ nm, we obtain $r_{ch} = 2340\ \Omega\,\mu\mathrm{m}^2$ and thus $r_s = 477\ \Omega\,\mu\mathrm{m}^2$. The NL spin-valve measurements for this device were performed at a RA product of 1675 $\Omega\,\mu\mathrm{m}^2$. This is a factor of 3.5 larger than r_s. The reduction of the spin signal due to back flow is then by a factor of 0.78. Taking this into account would increase the TSP for the device with 0.75 nm of MgO from 0.85% to 0.96%. A similar analysis for the device with 0.9 nm of MgO yields a spin signal reduction due to back flow by a factor of 0.94, with a corresponding correction of the TSP from 15% to 15.5%. Thus, even for the smallest MgO thicknesses, back flow does not play a significant role.

[1] J. S. Moodera, L. R. Kinder, T. M. Wong, and R. Meservey, Large Magnetoresistance at Room Temperature in Ferromagnetic Thin Film Tunnel Junctions, Phys. Rev. Lett. **74**, 3273 (1995).

[2] W. Butler, X.-G. Zhang, T. Schulthess, and J. MacLaren, Spin-dependent tunneling conductance of Fe|MgO|Fe sandwiches, Phys. Rev. B **63**, 054416 (2001).

[3] J. Mathon and A. Umerski, Theory of tunneling magnetoresistance of an epitaxial Fe/MgO/Fe(001) junction, Phys. Rev. B **63**, 220403(R) (2001).

[4] S. S. P. Parkin, C. Kaiser, A. Panchula, P. M. Rice, B. Hughes, M. Samant, and S. H. Yang, Giant tunneling magnetoresistance at room temperature with MgO (100) tunnel barriers, Nat. Mater. **3**, 862 (2004).

[5] S. Yuasa, T. Nagahama, A. Fukushima, Y. Suzuki, and K. Ando, Giant room-temperature magnetoresistance in single-crystal Fe/MgO/Fe magnetic tunnel junctions, Nat. Mater. **3**, 868 (2004).

[6] S. Yuasa and D. D. Djayaprawira, Giant tunnel magnetoresistance in magnetic tunnel junctions with a crystalline MgO(001) barrier, J. Phys. D: Appl. Phys. **40**, R337 (2007).

[7] C. Chappert, A. Fert, and N. Van Dau, The emergence of spin electronics in data storage, Nat. Mater. **6**, 813 (2007).

[8] L. Thomas *et al.*, Perpendicular spin transfer torque magnetic random access memories with high spin torque efficiency and thermal stability for embedded applications (invited), J. Appl. Phys. **115**, 172615 (2014).

[9] H. Sato, E. C. I. Enobio, M. Yamanouchi, S. Ikeda, S. Fukami, S. Kanai, F. Matsukura, and H. Ohno, Properties of magnetic tunnel junctions with a MgO/CoFeB/Ta/CoFeB/MgO recording structure down to junction diameter of 11 nm, Appl. Phys. Lett. **105**, 062403 (2014).

[10] K. Ando, S. Fujita, J. Ito, S. Yuasa, Y. Suzuki, Y. Nakatani, T. Miyazaki, and H. Yoda, Spin-transfer torque magnetoresistive random-access memory technologies for normally off computing (invited), J. Appl. Phys. **115**, 172607 (2014).

[11] S. Tsunegi, K. Yakushiji, A. Fukushima, S. Yuasa, and H. Kubota, Microwave emission power exceeding 10μW in spin torque vortex oscillator, Appl. Phys. Lett. **109**, 252402 (2016).

[12] A. Fukushima, T. Seki, K. Yakushiji, H. Kubota, H. Imamura, S. Yuasa, and K. Ando, Spin dice: A scalable truly random number generator based on spintronics, Appl. Phys. Express **7**, 083001 (2014).

[13] J. Torrejon, M. Riou, F. A. Araujo, S. Tsunegi, G. Khalsa, D. Querlioz, P. Bortolotti, V. Cros, K. Yakushiji, A. Fukushima, H. Kubota, S. Yuasa, M. D. Stiles, and J. Grollier, Neuromorphic computing with nanoscale spintronic oscillators, Nature (London) **547**, 428 (2012).

[14] S. Cardoso, P. P. Freitas, C. de Jesus, P. Wei, and J. C. Soares, Spin-tunnel-junction thermal stability and interface interdiffusion above 300°C, Appl. Phys. Lett. **76**, 610 (2000).

[15] J. Hayakawa, S. Ikeda, Y. M. Lee, F. Matsukura, and H. Ohno, Effect of high annealing temperature on giant tunnel magnetoresistance ratio of CoFeB/MgO/CoFeB magnetic tunnel junctions, Appl. Phys. Lett. **89**, 232510 (2006).

[16] S. Ikeda, J. Hayakawa, Y. Ashizawa, Y. M. Lee, K. Miura, H. Hasegawa, M. Tsunoda, F. Matsukura, and H. Ohno, Tunnel magnetoresistance of 604% at 300 K by suppression of Ta diffusion in CoFeB/MgO/CoFeB pseudo-spin-valves annealed at high temperature, Appl. Phys. Lett. **93**, 082508 (2008).

[17] H. Maehara, K. Nishimura, Y. Nagamine, K. Tsunekawa, T. Seki, H. Kubota, A. Fukushima, K. Yakushiji, K. Ando, and S. Yuasa, Tunnel magnetoresistance above 170% and resistance-area product of 1$\Omega\mu$m^2 attained by in situ annealing of ultra-thin MgO tunnel barrier, Appl. Phys. Express **4**, 033002 (2011).

[18] X. Jiang, R. Wang, R. M. Shelby, R. M. Macfarlane, S. R. Bank, J. S. Harris, and S. S. P. Parkin, Highly Spin-polarized Room-temperature Tunnel Injector for Semiconductor Spintronics using MgO(100), Phys. Rev. Lett. **94**, 056601 (2005).

[19] O. M. J. van 't Erve, A. T. Hanbicki, M. Holub, C. H. Li, C. P. Awo-Affouda, E. Thompson, and B. T. Jonker, Electrical injection and detection of spin-polarized carriers in silicon in a lateral transport geometry, Appl. Phys. Lett. **91**, 212109 (2007).

[20] O. M. J. van 't Erve *et al.*, Information processing with pure spin currents in silicon: spin injection, extraction, manipulation, and detection, IEEE Trans. Electron Devices **56**, 2343 (2009).

[21] T. Suzuki, T. Sasaki, T. Oikawa, M. Shiraishi, Y. Suzuki, and K. Noguchi, Room-temperature electron spin transport in a highly doped Si channel, Appl. Phys. Express **4**, 023003 (2011).

[22] M. Shiraishi, Y. Honda, E. Shikoh, Y. Suzuki, T. Shinjo, T. Sasaki, T. Oikawa, K. Noguchi, and T. Suzuki, Spin transport properties in silicon in a nonlocal geometry, Phys. Rev. B **83**, 241204(R) (2011).

[23] T. Sasaki, T. Suzuki, Y. Ando, H. Koike, T. Oikawa, Y. Suzuki, and M. Shiraishi, Local magnetoresistance in Fe/MgO/Si lateral spin valve at room temperature, Appl. Phys. Lett. **104**, 052404 (2014).

[24] M. Ishikawa, H. Sugiyama, T. Inokuchi, K. Hamaya, and Y. Saito, Spin transport and accumulation in n^+-Si using Heusler compound Co_2FeSi/MgO tunnel contacts, Appl. Phys. Lett. **107**, 092402 (2015).

[25] M. Ishikawa, T. Oka, Y. Fujita, H. Sugiyama, Y. Saito, and K. Hamaya, Spin relaxation through lateral spin transport in heavily doped n-type silicon, Phys. Rev. B **95**, 115302 (2017).

[26] A. Tiwari, T. Inokuchi, M. Ishikawa, H. Sugiyama, N. Tezuka, and Y. Saito, Room temperature observation of high spin polarization in post annealed $Co_2FeSi/MgO/n^+$-Si on insulator devices, Jpn. J. Appl. Phys. **56**, 04CD05 (2017).

[27] A. Spiesser, H. Saito, Y. Fujita, S. Yamada, K. Hamaya, S. Yuasa, and R. Jansen, Giant Spin Accumulation in Silicon Nonlocal Spin-Transport Devices, Phys. Rev. Appl. **8**, 064023 (2017).

[28] No data point was included for the sample with 0.75 nm of MgO, because a bias voltage of +840 mV would produce a too large current.

[29] A. Spiesser, H. Saito, Y. Fujita, S. Yamada, K. Hamaya, S. Yuasa, and R. Jansen, Spin signals in Si non-local transport devices with giant spin accumulation, Proc. SPIE **10357**, 103570C (2017).

[30] A. Fert and H. Jaffrès, Conditions for efficient spin injection from a ferromagnetic metal into a semiconductor, Phys. Rev. B **64**, 184420 (2001).

[31] R. Jansen, S. P. Dash, S. Sharma, and B. C. Min, Silicon spintronics with ferromagnetic tunnel devices, Semicond. Sci. Technol. **27**, 083001 (2012).

[32] A. Spiesser, Y. Fujita, H. Saito, S. Yamada, K. Hamaya, W. Mizubayashi, K. Endo, S. Yuasa, and R. Jansen, Quantification of Spin Drift in Devices with a Heavily Doped Si Channel, Phys. Rev. Appl. **11**, 044020 (2019).

[33] Unlike the schematic drawing in Fig. 1(a), the actual nonlocal devices consist of a Si strip of a few 100 μm in length, with *two* pairs of FM contacts, with a separation of about 30 μm between the two pairs. The resistivity of the channel was measured in a four-terminal geometry, using the two reference contacts at the ends of the channel for the current, and two FM contacts, one of each pair of FM contacts, to probe the voltage.

[34] G. Schmidt, D. Ferrand, L. W. Molenkamp, A. T. Filip, and B. J. van Wees, Fundamental obstacle for electrical spin injection from a ferromagnetic metal into a diffusive semiconductor, Phys. Rev. B **62**, R4790 (2000).

[35] E. I. Rashba, Theory of electrical spin injection: Tunnel contacts as a solution of the conductivity mismatch problem, Phys. Rev. B **62**, R16267 (2000).

[36] M. Julliere, Tunneling between ferromagnetic films, Phys. Lett. A **54**, 225 (1975).

[37] S. Yuasa, A. Fukushima, H. Kubota, Y. Suzuki, and K. Ando, Giant tunneling magnetoresistance up to 410% at room temperature in fully epitaxial Co/MgO/Co magnetic tunnel junctions with bcc Co(001) electrodes, Appl. Phys. Lett. **89**, 042505 (2006).

[38] P. Mavropoulos, Spin injection from Fe into Si(001): Ab initio calculations and role of the Si complex band structure, Phys. Rev. B **78**, 054446 (2008).

[39] Z. G. Yu and M. E. Flatté, Spin diffusion and injection in semiconductor structures: Electric field effects, Phys. Rev. B **66**, 235302 (2002).